THE JOURNAL OF PHYSICAL CHEMISTRY B

Article

pubs.acs.org/JPCB

Quantitative Nanoscale Analysis of IgE-FcεRI Clustering and Coupling to Early Signaling Proteins

Sarah L. Veatch,[†,‡] Ethan N. Chiang,[†,§] Prabuddha Sengupta,[∥] David A. Holowka, and Barbara A. Baird*

Department of Chemistry and Chemical Biology, Cornell University, Ithaca, New York 14853-1301, United States

Supporting Information

ABSTRACT: Antigen-mediated cross-linking of IgE bound to its receptor, FcεRI, initiates a transmembrane signaling cascade that results in mast cell activation in the allergic response. Using immunogold labeling of intact RBL mast cells and scanning electron microscopy (SEM), we visualize molecular reorganization of IgE-FcεRI and early signaling proteins on both leaflets of the plasma membrane, without the need for ripped off membrane sheets. As quantified by pair correlation analysis, we observe dramatic changes in the nanoscale distribution of IgE-FcεRI after binding of multivalent antigen to stimulate transmembrane signaling, and this is accompanied by similar clustering of Lyn and Syk tyrosine kinases, and adaptor protein LAT. We find that Lyn co-redistributes with IgE-FcεRI into clusters that cross-correlate throughout 20 min of stimulation. Inhibition of tyrosine kinase activity reduces the numbers of both IgE-FcεRI and Lyn in stimulated clusters. Coupling of these proteins is also decreased when membrane cholesterol is reduced either before or after antigen addition. These results provide evidence for involvement of FcεRI phosphorylation and cholesterol-dependent membrane structure in the interactions that accompany IgE-mediated activation of RBL mast cells. More generally, this SEM view of intact cell surfaces provides new insights into the nanoscale organization of receptor-mediated signaling complexes in the plasma membrane.

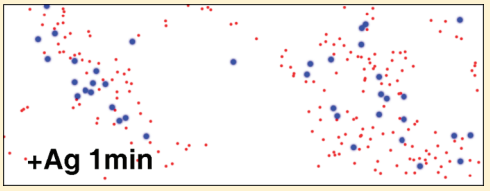

INTRODUCTION

Cross-linking of IgE bound to its high-affinity receptor, FcεRI, by multivalent antigen initiates a tyrosine kinase signaling cascade in mast cells that activates downstream signaling processes, including Ca^{2+} mobilization and exocytosis of secretory granules containing histamine and other mediators of the allergic response.[1] Triggered by IgE-FcεRI cross-linking, the Src family kinase Lyn rapidly phosphorylates immunoreceptor tyrosine-based activation motifs (ITAMs) on the β and γ subunits of FcεRI. These provide docking sites for recruitment of Lyn and Syk, respectively, that facilitate Syk kinase activation and consequent signal propagation.[2,3] Although receptor phosphorylation by Lyn is well established as the first enzymatic event following receptor aggregation,[4,5] the structural interactions that mediate this functional coupling within the plasma membrane remain ill-defined.[6,7]

Interactions between FcεRI and Lyn have been detected biochemically in several studies,[8,9] and a yeast two-hybrid study provided evidence that the unique domain of Lyn kinase binds weakly to the cytoplasmic segment of FcεRIβ in the absence of receptor phosphorylation.[10] Previous studies also established that the SH2 domain of Lyn binds to the phosphorylated ITAM of FcεRIβ to amplify FcεRI signaling.[11,12] A range of studies show that plasma membrane lipids that connect to the cytoskeleton are involved in regulating these interactions: Antigen cross-linking stabilizes association of IgE-FcεRI with cholesterol-dependent, ordered lipid membrane domains in the presence of active Lyn to initiate the tyrosine phosphorylation cascade.[13−15]

Despite this biochemical evidence for antigen-dependent interactions between Lyn and FcεRI that involves both proteins and membrane lipid domains, it has been difficult to detect co-redistribution of Lyn with clustered IgE-FcεRI using fluorescence microscopy under standard conditions for cell activation.[16,17] Fluorescence cross-correlation spectroscopy, as well as IgE-FcεRI engagement with patterned ligands, reveals stimulated interaction between Lyn and IgE-FcεRI, but these interactions are observed on the micrometer distance scale and occur more slowly than the nanoscale initiation of the tyrosine phosphorylation cascade.[17,18] Similarly, interactions between IgE-FcεRI and Syk or the key adaptor protein, LAT,[19] have been difficult to detect by fluorescence imaging methods under physiologically relevant conditions of antigen stimulation.[20]

Nanometer-scale resolution is needed to elucidate these interactions, and current developments in super resolution optical methods are showing great promise in overcoming the diffraction limit of UV and visible light.[21−24] Electron microscopy has proven successful over many years to resolve protein and membrane heterogeneity on the molecular level, and an established technique is to visualize immunogold-labeled protein distributions. Early studies from the Oliver laboratory used scanning electron microscopy (SEM) with backscatter detection (BSD) of immuno-gold particles to characterize the time-dependent clustering of IgE-FcεRI in

Special Issue: B: Harold A. Scheraga Festschrift

Received: January 6, 2012
Revised: March 2, 2012
Published: March 8, 2012

response to IgE-specific cross-linking on intact RBL mast cells.[25,26] More recently, several groups have used transmission electron microscopic analysis of ripped-off plasma membrane sheets from RBL cells and other cell types and have concluded that a variety of gold-labeled proteins in both leaflets appear clustered in resting cells when distributions are quantified using a modified Ripley's K function analysis. Using this approach, IgE-FcεRI, Lyn, Syk, and LAT have been reported to be self-clustered in membrane sheets derived from unstimulated RBL cells, and these proteins redistribute into larger clusters that only partly overlap in response to IgE-FcεRI cross-linking by antigen.[27,28]

Here, we show that SEM can be used to visualize immunogold particles bound to IgE-FcεRI and other proteins at both the outer and inner leaflets of the plasma membrane of the dorsal surface of intact RBL mast cells with nanometer resolution. We use secondary electron detection (SED) to image cell surface topology, together with BSD to image gold particle distributions. This approach eliminates the necessity of ripping off plasma membranes to visualize inner leaflet components, providing a less perturbing sample preparation for analysis of nanoscale interactions of signaling proteins. By quantifying measured gold particle distributions with pair auto- and cross-correlation functions, we identify experimental limitations, such as overcounting, and we extract physical parameters to describe protein clusters in the membrane, including average cluster size and average number of gold labeled proteins per cluster. With SEM we find that IgE-FcεRI, Lyn, Syk, and LAT are randomly distributed in unstimulated cells, and these proteins redistribute into large clusters within minutes of adding multivalent antigen to cross-link IgE-FcεRI and activate cells at 37 °C. Parallel SEM experiments reveal the complementary roles of cholesterol content and kinase-dependent protein−protein interactions at this earliest stage of cell signaling when FcεRI and Lyn reside in the same membrane domain. Our robust SEM imaging techniques with quantitative pair correlation analysis address previous uncertainties and provide new insights into the interactions of key signaling proteins and the role of plasma membrane structure during the earliest steps of immune cell signaling.

EXPERIMENTAL METHODS

Chemicals and Reagents. Rabbit anti-Alexafluor 488 (A488), A488-cholera toxin subunit B (A488-CTxB), and fluorescein isothiocyanate (FITC)-CTxB were purchased from Invitrogen (Eugene, OR). Rabbit anti-LAT was purchased from Upstate Biotechnology (Lake Placid, NY). Mouse anti-Lyn (H-6), rabbit anti-Lyn (44), and rabbit anti-Syk (N-19) were purchased from Santa Cruz Biotechnology (Santa Cruz, CA). Mouse mAb OX-7 (anti-Thy-1) was purchased from BDPharmingen (San Diego, CA). Glutaraldehyde (25% stock) was purchased from Ted Pella (Redding, CA). Paraformaldeyde was purchased from Electron Microscopy Services (Hatfield, PA). Mouse anti-FITC, Mouse anti-green fluorescent protein (GFP) (and yellow fluorescent protein (YFP)), 10 nm gold-conjugated antirabbit IgG (whole molecule), 10 nm gold-conjugated antimouse IgG (whole molecule), 5 nm gold-conjugated antirabbit IgG (whole molecule), and methyl-β-cyclodextrin (MβCD) were purchased from Sigma (St. Louis, MO). Five-nanometer gold-conjugated antimouse was purchased from GE Healthcare (Piscataway, NJ). PP1 was purchased from Biomol (Plymouth Meeting, PA). A488-IgE was prepared by conjugating purified mouse monoclonal anti-2,4-dinitrophenyl (DNP) IgE with A488 (Invitrogen) as previously described.[14,17] Vectors containing complementary DNA (cDNA) for YFP-GT46 and YFP-GL-GPI were provided by J. Lippincott-Schwartz (NIH, Bethesda, MD) and A. Kenworthy (Vanderbilt University School of Medicine, Nashville, TN), respectively, and the plasmids encoding monomeric YFP-GL-GPI and monomeric YFP-GT46 were constructed from YFP-GL-GPI and YFP-GT46 by introducing the A206K mutation,[29] as described previously.[30]

Cell Culture and SEM Sample Preparation. RBL-2H3 mast cells were grown overnight to ∼50% confluency on 2 mm × 2 mm silicon chips at 37 °C under standard cell culture conditions,[18] and high affinity IgE receptors (FcεRI) were labeled with A488-IgE (1 μg/mL) for 2−3 h prior to the experiment. To stimulate cells, IgE-FcεRI was cross-linked with multivalent antigen (DNP-BSA (BSA = bovine serum albumin), 1 μg/mL) at 37 °C in culture medium for specified times, washed quickly in phosphate-buffered saline (PBS), and immediately fixed in 4% (w/v) *p*-formaldehyde and 0.1% (w/v) glutaraldehyde for 10 min at room temperature in PBS. For some experiments, cells were preincubated for 5 min at 37 °C with either 10 mM MβCD or 4 μM PP1 prior to addition of antigen, or cells were incubated for 5 min at 37 °C with 10 mM MβCD after 1 min of stimulation by antigen. Fixed cell samples were washed in blocking solution (2 mg/mL BSA and 2% (v/v) fish gelatin in PBS) and labeled sequentially with primary antibodies and gold conjugated secondary antibodies in the presence (usual) or absence (control) of 0.1% Triton X-100 in blocking solution. Each incubation was 1 h at room temperature with wash steps in between.

For single-label experiments, the primary antibodies were anti-A488 pAb, anti-Lyn pAb, anti-Syk pAb, or anti-LAT pAb, and the 10 nm gold conjugated secondary antibody was goat antirabbit IgG. For the Thy1 single-label experiment, the primary antibody was anti-Thy1 mAb (Ox7), and the 10 nm gold conjugated secondary antibody was goat antimouse IgG. For double label experiments, samples were labeled first with 10 nm and then 5 nm gold antibody conjugates. For double label IgE (5 nm) and Lyn (10 nm), primary antibodies were anti-A488 pAb and anti-Lyn mAb (H-6), and gold conjugated secondary antibodies were 10 nm goat antimouse IgG and 5 nm goat antirabbit IgG. For double-label IgE (10 nm) and Thy-1 (5 nm) experiments, primary antibodies were anti-A488 pAb or anti-Thy1 mAb (Ox7), and gold conjugated secondary antibodies were 10 nm goat antirabbit IgG or 5 nm goat antimouse IgG. After labeling with primary and gold-conjugated secondary antibodies, the cell samples were further fixed in 4% *p*-formaldehyde and 1% gluteraldehyde for 5 min at room temperature, and then thoroughly washed in distilled water. Following dehydration through a series of graded ethanol washing steps, samples were critical-point-dried, mounted on round aluminum SEM stubs, and sputtered with carbon to prevent charging.

Preparation of Immobilized Gold-Antibody Conjugates on Silicon Surface. Following plasma-treatment, silica chips were immersed in a 2% (3-aminopropyl)trimethoxysilane (APTMS) solution in acetone for 10 min, then thoroughly washed with acetone and PBS. These amino-functionalized surfaces were then treated with 0.1% glutaraldehyde (in PBS) for 30 min at room temperature, followed by 1 h incubation at room temperature with either 10 μg/mL or 50 μg/mL A488-IgE (10 μg/mL shown in Figure 2a) or 10 μg/mL anti-Lyn. A488-proteins immobilized on these surfaces were labeled with

Table 1. Counting Statistics for Gold Particle Analysis[a]

	−Ag		+Ag 1 min		+Ag 5 min		+Ag 10 min		+Ag 20 min	
single label	N_{tot}	ρ 1/μm^2	N_{tot}	ρ 1/μm^2	N_{tot}	ρ 1/μm^2	N_{tot}	ρ 1/μm^2	N_{tot}	ρ 1/μm^2
FcεRI (10 nm)	185054	260	105159	138	23979	155	13331	86	3430	26
Lyn (10 nm)	10558	30	23664	28	2180	30	5419	27	4200	25
Syk (10 nm)	9500	29	14874	32	4240	33	1816	8	2454	10
LAT(10 nm)	6556	19	7240	20	2982	17	3963	16	2394	12
double label										
FcεRI (5 nm)	11632	214	7966	135	1566	80	297	42	230	20
Lyn (10 nm)	1053	19	991	17	356	18	42	6	98	9

[a]An extensive data set of surface bound immuno-gold particles is used to compute the correlation functions presented in this study. N_{tot} is the total number, and ρ is the average density of gold particles identified for each experimental condition. Typically, labeling efficiency is reduced in double-labeling experiments, especially for the 10 nm gold, which labels Lyn in these studies.

primary and gold-conjugated secondary antibodies and prepared for SEM imaging as described above for cell samples.

Electron Microscopy and Imaging Statistics. Mounted samples were imaged with a Schottky field emission scanning electron microscope (LEO 1550) at 20KeV. The dorsal (top) surfaces of intact, adherent cells were imaged using secondary electron detection (SED) and backscatter detection (BSD) at high magnification. Flat membrane regions were selected for imaging. For single-label experiments, 10 nm gold particles were used, and individual micrographs were obtained at 35K magnification, typically imaging 2.4 μm^2 of the cell surface. For double label experiments, 10 nm and 5 nm gold particles were used, and micrographs were obtained at either 75 K or 100 K magnification. The positions of both 5 nm and 10 nm gold particle centers were identified using automated image processing algorithms and a weighted centroid approach, and differently sized particles were distinguished by establishing cutoffs in centroid intensity and integrated intensity. Image processing methods are described in more detail in the Supporting Information and Supplemental Figure S1. Immuno-gold labeled protein distributions for many different cells and many experiments were obtained for all experimental conditions presented. The total number of gold particles, total area imaged, and gold-labeled densities for samples analyzed in this study are summarized in Table 1.

Pair Correlation Function Analysis. For single-label experiments, pair autocorrelation functions, $g(r)$, were evaluated by computing the autocorrelation of a reconstructed image of gold particle centers. For double-label experiments, pair cross-correlation functions, $c(r)$, were evaluated by computing the cross-correlation between two images of gold particle centers. Both autocorrelation and cross-correlation functions are normalized to 1 at large radius (the dimensions of the SEM image, $r \gg 250$ nm). By this definition, correlation functions quantify the probability of finding a second particle a distance r away from a given particle, and a value of 1 indicates that particles are randomly distributed at that distance. This probability can be converted to an average density of gold particles within a ring of radius r and width dr from a given particle by multiplying by the average gold particle density, ρ, obtained by summing all gold particles identified and dividing by the total large imaged area.

Pair auto- and cross- correlation functions were tabulated in Matlab (Mathworks, Natick, MA) using fast Fourier transforms (FFTs) as follows:

$$g(\vec{r}) = \frac{\mathrm{FFT}^{-1}(|\mathrm{FFT}(I)|^2)}{\rho^2 N(\vec{r})}$$

where FFT^{-1} is an inverse fast Fourier transform, I is a binary image where pixels have a value of 1 at gold particle centers and all other pixels have a value of 0, and $N(\vec{r})$ is a normalization that accounts for the finite size of the acquired image. The image I is padded with zeros in both directions out to a distance larger than the range of the desired correlation function (maximally the size of the original image) to avoid artifactual correlations due to the periodic nature of FFT functions. The normalization factor N is the autocorrelation of a window function W that has a value of 1 inside the measurement area, and is also padded by an equal number of zeros:

$$N(\vec{r}) = \mathrm{FFT}^{-1}(|\mathrm{FFT}(W)|^2)$$

This normalization accounts for the fact that there are fewer possible pairs separated by large distances due to the finite image size.

Cross-correlation functions between images of 5 nm and 10 nm particle centers (I_{5nm} and I_{10nm}, respectively) are tabulated in a similar manner:

$$c(\vec{r}) = \mathrm{Re}\left\{\frac{\mathrm{FFT}^{-1}(\mathrm{FFT}(I_{5nm}) \times \mathrm{conj}(\mathrm{FFT}(I_{10nm}))}{\rho_{5nm}\rho_{10nm}N(\vec{r})}\right\}$$

Here conj(...) indicates a complex conjugate, ρ_{5nm} and ρ_{10nm} are the average surface densities of 5 nm and 10 nm particles. respectively, and Re{...} indicates the real part. This computation method of tabulating pair auto- and cross-correlations is mathematically identical to brute force averaging methods.

Correlation functions were angularly averaged by first converting to polar coordinates using the Matlab command *cart2pol* and then binning by radius. Values for $g(r)$ are obtained by averaging $g(\vec{r})$ values that correspond to the bins assigned in terms of radius. Errors in $g(r)$ are standard errors of the mean.

Autocorrelation functions for radii greater than 50 nm and cross-correlation functions for radii greater than 10 nm are well fit by single exponentials:

$$g(r) = 1 + A\exp\{-r/\xi\}$$

dx.doi.org/10.1021/jp300197p | J. Phys. Chem. B 2012, 116, 6923−6935

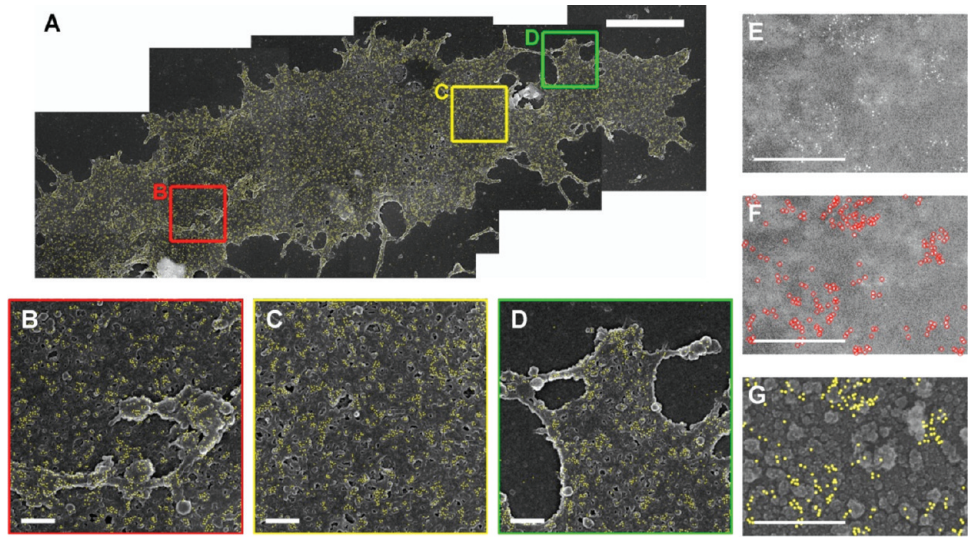

Figure 1. Cell surface topography and immuno-gold distribution is visualized with SEM. (A) Composite SED image of the dorsal surface on intact RBL cells. Immuno-gold particles (10 nm) labeling IgE-FcεRI are superimposed in yellow; particle centers are determined using BSD in conjunction with automated image processing. Images are acquired at 15K magnification, and scale bar is 5 μm. (B–D) Higher magnification images from panel A in areas indicated; scale bars are 500 nm. (E–G) SEM images acquired at higher magnification (35K) for increased lateral resolution and for automated identification of gold particle location; scale bars are 500 nm. (E) Raw BSD image. (F) Gold particle centers identified from BSD micrographs with automated image processing algorithms (Supplemental Figure S1). Apparent topology in E–G arises from carbon coating and is uncorrelated with gold image processing. (G) Reconstructed particle centers overlaid on SED distributions.

where A and ξ represent intensity of clustering and characteristic correlation distance, respectively. The average number of gold particles per cluster N_{cl} is given by

$$N_{cl} = 1 + \rho \int_{\infty}^{0} (g(r) - 1) \times 2\pi r \, dr \approx 2\pi A \xi^2 \rho$$

We define the increased protein density in clusters to be

$$\rho_{cl}/\rho = N_{cl}/\left(\pi \xi^2 \rho\right) \approx 2A$$

Simulations of IgE-FcεRI and Lyn Distributions in Figure 7. Random field Ising models with a conserved order parameter were simulated as described in ref 31 with minor modifications. Monte Carlo simulations were conducted on a square lattice with periodic boundary conditions; objects at individual lattice sites interact with only their four nearest neighbors. Updates satisfy detailed balance and were accomplished through nonlocal component swaps to improve equilibration times. The vast majority of components in simulations represent generic ordered components (orange pixels) or disordered components (white pixels). Like components have favorable (+1) interactions with their nearest neighbors; unlike components have unfavorable (−1) interactions with nearest neighbors. Within this scheme the temperature is calibrated so that physiological temperature (37 °C) corresponds to 1.04 times the two-dimensional (2D) Ising model critical temperature of $T_c = 2/\ln(1 + \sqrt{2})$. The calibration of temperature is based on our previous observations of micrometer-scale critical fluctuations in isolated plasma membrane vesicles near room temperature.[32]

Simulations also contain pixels representing IgE-FcεRI and Lyn components. IgE-FcεRI distributions are taken directly from SEM images and remain fixed throughout the simulation, and IgE-FcεRI has favorable (+1) interactions with neighboring orange pixels and unfavorable interactions (−1) with neighboring white pixels. Lyn components also have favorable interactions (+0.5) with orange pixels and unfavorable interactions with white pixels (−0.5), and are allowed to move freely throughout the lattice. Interactions between Lyn and IgE-FcεRI pixels depend on the local lipid environment. When Lyn is surrounded by disordered (white) pixels, Lyn and IgE-FcεRI pixels interact with weak but favorable interactions (+1). Lyn and IgE-FcεRI pixels have much stronger interactions (+10) when Lyn is surrounded by ordered (orange) pixels. This interaction energy is intended to roughly represent the estimated binding constant of $K = 2.5 \times 10^{-6}$ molecules^{-1}, as $\ln(K) \approx 10$, for activated Lyn binding to a phosphorylated ITAM region on FcεRI.[33] The probability of this stronger binding with IgE-FcεRI scales linearly with the number of ordered neighbors for cases where Lyn is surrounded by IgE-FcεRI and either one or two ordered components. The interactions are constrained such that only one strong binding interaction can occur for each IgE-FcεRI at a given time.

Simulations mimicking PP1 treatment are conducted by removing the strong binding state between IgE-FcεRI and Lyn so that these components can only interact with an energy of +1. Simulations mimicking cholesterol depletion are conducted by increasing the number of disordered (white) pixels, such that 85% of pixels are white. Correlation functions curves were calculated from 200 snapshots from the same simulation and averaged for each condition.

RESULTS

Visualizing Plasma Membrane Lateral Heterogeneity by SEM. We directly visualize protein heterogeneity on the dorsal surface of intact RBL cells using high-resolution SEM with a combination of SED and BSD, as illustrated in Figure 1. SED is sensitive to topography and allows identification of flat cell surfaces to avoid membrane structures that can alter the appearance of protein organization (compare panels B and C in Figure 1). Protein distributions in the cell membrane are determined by imaging distributions of specific gold labels with

dx.doi.org/10.1021/jp300197p | J. Phys. Chem. B 2012, 116, 6923–6935

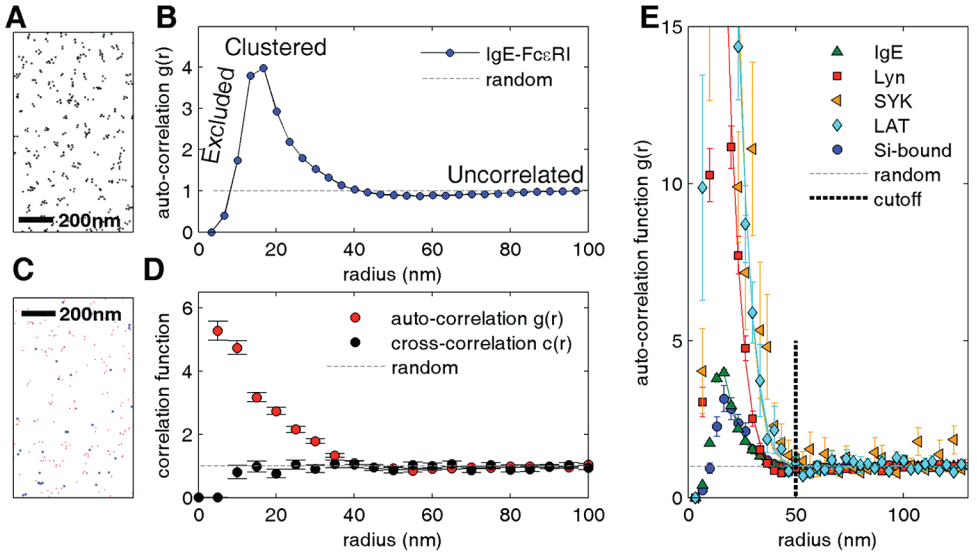

Figure 2. Gold particles labeling proteins are self-clustered in resting cells. (A) Clustering is evident in representative reconstructed SEM (BSD) images of gold particles that label IgE bound to the receptor FcεRI. (B) Pair autocorrelation functions of gold particle distributions from many images quantify immuno-gold labeled IgE-FcεRI in the plasma membrane. (C,D) Double label experiments indicate that self-clustering of golds labeling IgE-FcεRI complexes is dominated by multiple gold particles binding to single target proteins. (C) Images of A488- or FITC-conjugated IgE-FcεRI that are distinctively immuno-labeled with 5 nm (red) and 10 nm (blue) gold particles, respectively. (D) Autocorrelation functions of 5 nm particles (red points) indicate self-clustering. By contrast, the cross-correlation function for the 5 nm vs 10 nm particles is 1 within error bounds at all r (black points). The presence of significant self-clustering (red points) in the absence of co-clustering (black points) indicates that overcounting of multiple gold binding to individual target proteins dominates observations of self-clustering in this single label experiment. (E) Correlation functions, $g(r)$ vs r, are evaluated and averaged over many images of specified target proteins (Table 1) and indicate that gold particles are significantly self-clustered at short distances in all cases. In subsequent figures, we only show correlation functions for $r > 50$ nm to avoid any self-clustering artifacts associated with multiple labels bound to single target proteins.[35] The correlation curves in (E) are fit for $r > 10$ nm by Gaussian functions centered at $r = 0$.

BSD at high magnification and by applying automated image processing and gold particle identification algorithms to determine particle coordinates for reconstructed images as described in the Supporting Information (Figure S1) and illustrated in Figure 1E−G. Our SEM method detects both outer and inner leaflet gold-labeled proteins following fixation and labeling in the presence of Triton X-100. Plasma membrane-associated proteins are specifically labeled with the standard approach of primary antibodies followed by gold-conjugated secondary antibodies, and little to no background binding occurs on the bare silicon surface (Figure 1D). Sample preparation and controls are described in the Experimental Methods section and in the Supporting Information (Figure S2).

Quantifying Protein Distributions from SEM Micrographs. Figure 2A shows a representative, reconstructed BSD-SEM image specifying cell surface distributions of 10 nm gold-labeled IgE-FcεRI in an unstimulated cell. For efficient labeling of IgE postfixation, we use Alexa488-conjugated IgE prebound to FcεRI and rabbit anti-Alexa488 antibody as the primary antibody. We find average surface densities (ρ) of ∼260 gold particles/μm^2 (Table 1). This value is consistent with previous measurements of FcεRI surface density in live RBL cells[34] and indicates a high average labeling efficiency of about 1 gold particle per IgE-FcεRI. Our labeling scheme allows multiple labels binding to individual IgE, and this average means that some IgE are labeled with more than one gold particle and some with none. Gold particles labeling IgE-FcεRI appear clustered in resting cells (Figure 2A), and we chose to characterize the clustering by evaluating pair correlation functions. The pair autocorrelation, $g(r)$, quantifies the increased probability of finding a second gold particle a distance r away from any given particle, and is calculated as described in the Experimental Methods. The pair autocorrelation curve derived from many (80) images of gold particles labeling cell surface IgE-FcεRI is shown in Figure 2B. We find that $g(r)$ values trend toward 1 at long radii ($r > 50$ nm), indicating that these gold labels are randomly distributed and thereby are not correlated at these distances. At very short radii ($r < 10$ nm), $g(r)$ values fall below 1 because gold particles cannot pack more tightly than their hard sphere radius and thus are excluded. The $g(r)$ values are greater than 1 for radii between ∼10 and ∼40 nm, indicating that there is an increased probability of finding pairs of gold particles separated by these distances than would be expected in a random distribution ($g(r) = 1$; dashed line in Figure 2B). For example, $g(20\text{nm}) \approx 4$ means that it is roughly 4 times more likely to find two gold particles separated by 20 nm than is expected from a random distribution. This also means that the average density of gold particles 20 nm away from any given particle is 4 times greater than the overall average surface density.

Because the standard labeling scheme uses primary and secondary antibodies to bind gold particles to target proteins, apparent self-clustering may arise when multiple gold particles label single target proteins. We previously described a method to estimate the magnitude of this short-range, apparent clustering due to overcounting of labels.[35] We find that $g(r)$ curves for all the target proteins investigated in this study are consistent with the same model,[35] after determining an average labeling efficiency close to 1 gold per accessible target protein (Supporting Information, Figure S3A). For the case of IgE-FcεRI, we confirmed that multiple gold labels dominates the

dx.doi.org/10.1021/jp300197p | J. Phys. Chem. B 2012, 116, 6923−6935

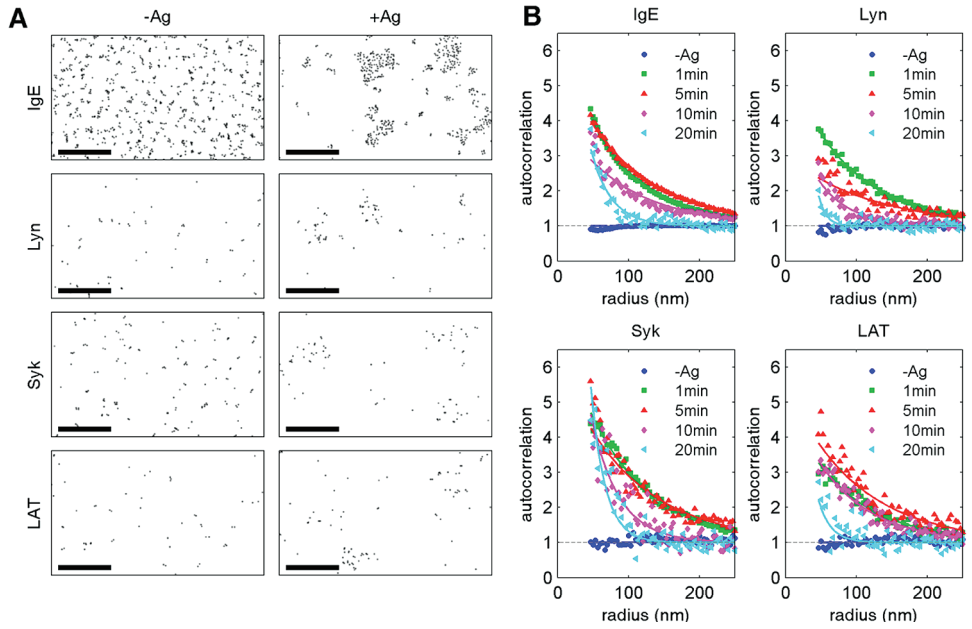

Figure 3. IgE-FcεRI, Lyn, Syk, and LAT rapidly redistribute into large clusters after addition of antigen to cross-link IgE-FcεRI, and clusters decrease in size over 20 min. (A) Representative reconstructed BSD images of plasma membrane with immuno-gold labeling of specified target proteins (10 nm gold particles). Left panels: SEM samples prepared from cells incubated at 37 °C in the absence of stimulus; right panels: SEM samples prepared from cells stimulated with antigen for 1 min at 37 °C. Scale bars are 500 nm. (B) Gold particle distributions are quantified for multiple images (N > 100; Table 1) using pair autocorrelation functions. Correlation curves are well fit by a single exponential for r > 50 nm. Extracted fit parameters are plotted in Figure 4, and those for IgE-FcεRI and Lyn are tabulated in Supplemental Table S1A.

apparent self-clustering by evaluating cross-correlation functions between two distinguishably labeled, yet functionally identical, pools of IgE- FcεRI complexes.[35] Similar to autocorrelation, the cross-correlation function, $c(r)$, quantifies the increased probability of finding a distinguishable particle a distance r away from a given particle of a different type. Unlike the autocorrelation function, $c(r)$ for proteins with distinctive labels is not altered by overcounting multiply labeled proteins.[35] For cross-correlation analysis, two separate pools of FcεRI were created by preincubating the cells with a mixture of IgE labeled with either the fluorophore Alexa488 or the fluorophore FITC prior to fixation in our standard procedure. These were distinctively labeled with fluorophore-specific primary antibodies of different species followed by species-specific secondary antibodies conjugated to gold particles of different sizes (Figure 2C). By this scheme, small and large gold particles cannot bind to the same FcεRI protein because only a single IgE antibody binds to each FcεRI protein.[36] Cross-correlation functions of the doubly labeled IgE-FcεRI (black points in Figure 2D) indicate random distributions within experimental error bounds ($c(r)$ = 1). This contrasts with autocorrelation of one population of gold labels (red points in Figure 2D), which shows clustering at short distances ($g(r)$ >1). The comparison confirms that the appearance of clustering in the images of IgE-FcεRI in unstimulated cells (Figure 2A) is due to multiple gold particles binding to single target proteins.

Autocorrelation functions for all proteins examined in resting cells follow the same general shape as found for IgE-FcεRI, although they vary in peak amplitude as shown in Figure 2E. A similar curve is obtained for Alexa488-IgE covalently coupled to silica, which was evaluated because it is expected to represent a random distribution. Our results reveal the pitfall of misinterpreting clustered gold particles at short distances for actual self-clustering of target proteins if multiple labels is a possibility. Therefore, to evaluate protein clustering, we chose to examine only correlations that persist beyond a radius of 50 nm, which is larger than the dimensions of bound primary and secondary antibodies in the gold immuno-labeling scheme (Supplemental Figure S3). On the basis of these results and our recent study, we expect that correlations for radii greater than 50 nm quantify the lateral organization of target proteins and are not significantly affected by the labeling efficiency of gold particles or finite size of labeling antibodies.[35] As can been seen in Figure 2E for unstimulated cells, autocorrelation functions for all proteins examined in our study are randomly distributed at distances beyond this cutoff value ($g(r$ > 50 nm) ∼ 1).

Protein Redistribution during Signaling. To probe the lateral organization of IgE-FcεRI and other proteins that participate in early signaling events, we imaged the distributions of IgE-FcεRI, Lyn kinase, Syk kinase, and LAT before and after stimulation with multivalent antigen at 37 °C (Figure 3A). The transmembrane receptor complex A488-IgE-FcεRI was visualized on the extracellular dorsal surface, and the signaling proteins Lyn, Syk, and LAT were labeled with antibodies specific for cytoplasmic epitopes and visualized at the same dorsal membrane. As represented by images in Figure 3A (left panels), immunogold-labeled IgE-FcεRI, Lyn, Syk, and LAT in unstimulated cells appear to be distributed in small clusters (r < 50 nm) at the plasma membrane. However, as described above, this apparent clustering cannot be distinguished from multiple gold labels on single target proteins. Pair autocorrelation functions for all of these proteins are shown in Figure 3B for unstimulated cells and for cells stimulated with antigen to cross-link IgE-FcεRI for indicated times ranging from 1 to 20 min at 37 °C. In all cases, the autocorrelation functions were evaluated from many images of cells, and the curves were truncated for $g(r$ < 50 nm) to avoid clustering arising from overcounting. For reference, Supplemental Figure S3B shows representative

dx.doi.org/10.1021/jp300197p | J. Phys. Chem. B 2012, 116, 6923−6935

correlation function curves for clustered protein distributions including points $r < 50$ nm. Beyond this distance, each of IgE, Lyn, Syk, and LAT is observed to be randomly distributed in unstimulated cells by autocorrelation analysis (Figure 3B; −Ag, blue circles).

Following cell stimulation by antigen for 1 min, labeled IgE-FcεRI complexes appear tightly packed in large clusters, consistent with antigen cross-linking and with previous SEM studies[25] (Figure 3A, top right panel). The signaling proteins Lyn kinase, Syk kinase, and LAT also redistribute into clusters of similar dimensions as those of the cross-linked IgE-FcεRI under these same conditions of antigen stimulation (Figure 3A, right panels), and each becomes highly autocorrelated at long distances ($g(r) > 1$ for $r > 50$ nm) within 1 min after addition of antigen (Figure 3B, green squares). The autocorrelation curves verify the visual observations represented in Figure 3A (right panels) that stimulated clusters range in size, but can be as large as 250 nm in radius. Autocorrelation curves evaluated from samples with longer periods of stimulation (5, 10, and 20 min) show that IgE-FcεRI and the three signaling proteins investigated sustain clustering for more than 10 min, although clusters become smaller with longer stimulation times. At 20 min of stimulation, autocorrelation curves decay more steeply such that $g(r) \sim 1$ for $r \geq \sim 100$ nm (Figure 3B, cyan triangles).

We found that the autocorrelated data shown in Figure 3B are fit well by the single exponential function $g(r) = 1 + A \exp\{-r/\xi\}$ for $r > 50$ nm, where the fit parameters ξ and A provide a quantitative measure of the size and the intensity of clustering, respectively. Several properties of clusters can be extracted from these fit parameters (Experimental Methods), and these are plotted in Figure 4 for the experiments in Figure 3B and also for parallel experiments carried out with Thy-1. Figure 4A shows cluster radius, represented by the correlation length, ξ, as a function of stimulation time. Within 1 min of antigen addition, all of the labeled IgE-FcεRI, Lyn, Syk, and LAT form large clusters (ξ = 70−90 nm) that gradually decrease in size (to $\xi \sim 20$ nm) during 20 min of stimulation. By contrast, the GPI-linked protein Thy-1 does not exhibit significant clustering either before or after cross-linking IgE-FcεRI with multivalent antigen under the same conditions. As shown in Figure 4B, the average number of gold particles labeling IgE-FcεRI, Lyn, Syk, and LAT proteins per cluster (N_{cl}) follows similar trends in time: N_{cl} increases rapidly during the first 1−5 min of antigen stimulation and decreases at longer stimulation times. If these proteins are co-clustered and they are labeled with gold-conjugated antibodies with the same efficiency, then the relative values of N_{cl} for these proteins indicate their corresponding stoichiometries.

The average surface density of gold particles labeling target proteins (ρ) varies with stimulation time, as shown in Figure 4C. The value of ρ for IgE-FcεRI declines by ∼50% during the first 10 min of stimulation consistent with cross-link-dependent internalization.[37] The value of ρ for Syk also declines during this initial stimulation period, consistent with stimulation-dependent internalization of Syk.[38] Alternatively, Syk may dissociate and return to the cytoplasm as IgE internalizes. By contrast, ρ for each of Lyn, LAT, and Thy-1 remains constant throughout the time course of stimulation, suggesting that these do not cointernalize with cross-linked IgE-FcεRI. We note that values for ρ may under-represent surface exposed target proteins if steric hindrance reduces immuno-gold labeling at higher densities of target proteins in clusters.

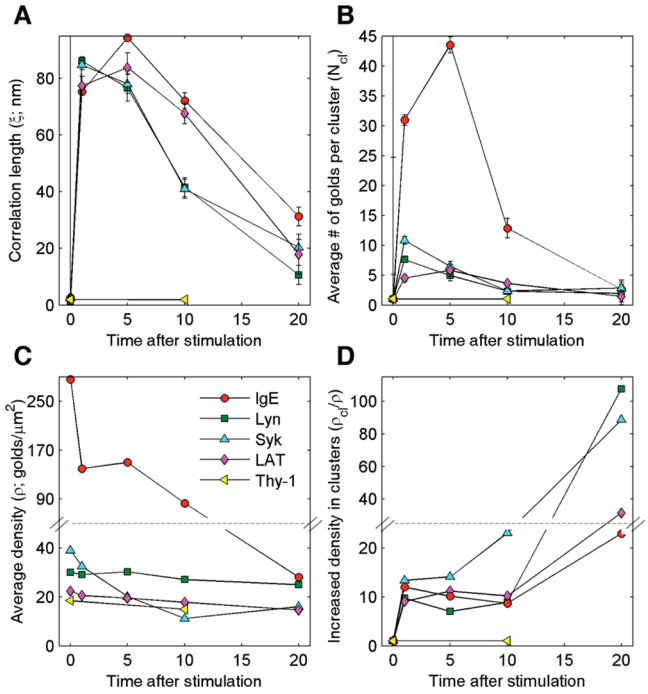

Figure 4. Physical properties of clustered target proteins as a function of stimulation time are measured or extracted from correlation functions. Autocorrelation functions determined from many images of specified target proteins are well fit to a single exponential as shown in Figure 3B, and parameters are determined as described in the text: correlation length, ξ (A); average number of gold particles per cluster, N_{cl} (B); average surface density, ρ (C); increased density of gold particles within clusters, ρ_{cl}/ρ (D). These parameters for IgE-FcεRI and Lyn are tabulated in Supplemental Table S1A.

The parameter ρ_{cl}/ρ provides a measure for the increased local density of gold particles within clusters. For gold particles labeling IgE-FcεRI, Lyn, Syk, and LAT (but not Thy-1), ρ_{cl}/ρ increases ∼10-fold during the first minute of stimulation, then more gradually continues to increase throughout the subsequent 20 min stimulation time course (Figure 4D). These results reveal that the membrane protein interactions within signaling clusters continue to change as stimulation progresses. Our findings that cluster sizes and enhanced densities of the signaling proteins change in parallel suggest that the signaling proteins examined are clustered within the same membrane domains.

Co-localization of IgE-FcεRI and Lyn Kinase in Double-Label Experiments. To determine directly whether Lyn co-redistributes with cross-linked IgE-FcεRI clusters or Lyn forms separate clusters, we double labeled these two proteins with distinguishable (5 nm and 10 nm) gold particles before and after stimulation with multivalent antigen at 37 °C. As represented in Figure 5A, we find that Lyn is visibly co-clustered with cross-linked IgE-FcεRI after 1 min of stimulation with antigen, and these two proteins remain co-clustered at longer stimulation times. By contrast, Thy-1 does not visibly co-redistribute with cross-linked IgE-FcεRI clusters under these conditions. Cross-correlation functions for IgE-FcεRI with Lyn and for IgE-FcεRI with Thy-1 are shown in Figure 5B. Similar to autocorrelation functions, cross-correlation functions from stimulated cells are fit well by a single exponential function, $c(r) = 1 + A \exp\{-r/\xi_c\}$ for $r > 10$ nm; where ξ_c corresponds to the

dx.doi.org/10.1021/jp300197p | J. Phys. Chem. B 2012, 116, 6923−6935

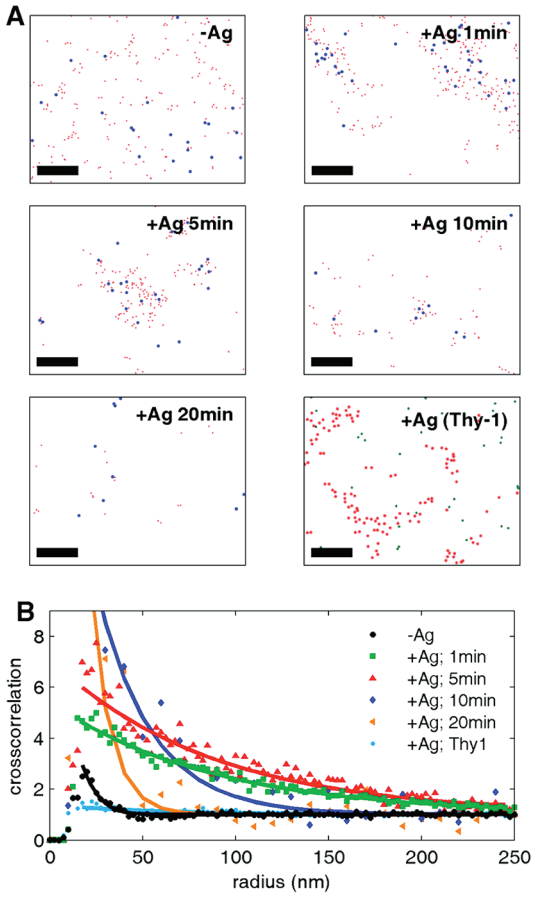

Figure 5. Double-label experiments reveal that Lyn, but not Thy-1, co-redistributes with IgE-FcεRI after cells are stimulated with antigen. (A) Representative reconstructed BSD images from cells that were stimulated (or not) for times indicated and specified target proteins were immuno-gold labeled. IgE-FcεRI (5 nm gold particles) and Lyn (10 nm gold particles) were double labeled, or IgE-FcεRI (10 nm gold particles) and Thy-1 (5 nm gold particles) were double labeled. Scale bars are 200 nm. (B) Gold particle distributions for many images from double label experiments represented in (A) are quantified using cross-correlation functions, and curves are well fit by an exponential. Extracted fit parameters for IgE-FcεRI and Lyn are tabulated in Supplemental Table S1B.

correlation length of the co-cluster. Fit parameters are reported in Supplemental Table S1B.

Although individual IgE-FcεRI appear randomly distributed in unstimulated cells (not self-cross-correlated in Figure 2D), and self-clustering of Lyn cannot be distinguished from multiple gold labeling of individual proteins (Figure 2E), we found that these two proteins cross-correlate with each other to a small degree at short distances (Figure 5B, black circles; ξ_c < 10 nm), indicating some tendency to preassociate in the absence of cross-linking by antigen. The average number of one labeled protein that is co-localized with the average second labeled protein can be estimated by integrating the cross-correlation function. For example, the average number of gold particles labeling IgE-FcεRI complexes co-localized with an average Lyn is given by $N_{\mathrm{cl-IgE\text{-}Fc\varepsilon RI}} = \rho_{\mathrm{IgE\text{-}Fc\varepsilon RI}} \sum_0^{r_{\max}}(c(r) - 1)2\pi r_i \Delta r_i$, where Δr_i is the short distance interval between adjacent points and $\rho_{\mathrm{IgE\text{-}Fc\varepsilon RI}}$ is the average surface density of gold particles labeling IgE-FcεRI proteins reported in Figure 4C (260 μm^{-2}). To minimize errors at large r, we included $c(r) - 1$ versus r points measured over the range of significant correlations (from r = 0 through $r_{\max}$ = 100 nm). This summation yields an average number of gold particles labeling FcεRI receptors that co-localize with an average Lyn, $N_{\mathrm{cl-IgE\text{-}Fc\varepsilon RI}} = 0.7 \pm 0.1$. If we instead evaluate the number of gold particles labeling Lyn proteins that are in close proximity to the average IgE-FcεRI, we obtain $N_{\mathrm{cl-Lyn}} = \rho_{\mathrm{Lyn}} \sum_0^{r_{\max}}(c(r) - 1)2\pi r_i \Delta r_i = 0.08 \pm 0.01$, using the average surface density of gold particles labeling Lyn reported in Figure 4C (30 μm^{-2}). If our labeling efficiency is close to 1 gold particle per target protein, then these numbers also describe the number of co-localized IgE- FcεRI complexes per average labeled Lyn and vice versa.

We can also deduce the fraction of labeled IgE-FcεRI and Lyn found in co-clusters from these data if we make the additional assumption that IgE-FcεRI and Lyn associate in a 1:1 complex. If this is the case, then the total number of IgE-FcεRI complexes and Lyn proteins in co-clusters will be the same. Above we calculated that the number of co-localized IgE-FcεRI complexes per labeled Lyn is $N_{\mathrm{cl-IgE\text{-}Fc\varepsilon RI}} = 0.7$. If the number of IgE-FcεRI complexes in co-clusters is the same as the number of Lyn proteins in co-clusters, then we can deduce that the number of co-clustered Lyn per total Lyn is also approximately 0.7, or 70% of total Lyn is preclustered with IgE-FcεRI. We also calculated that the average number of co-clustered Lyn proteins per IgE-FcεRI is $N_{\mathrm{cl-Lyn}} = 0.08 \pm 0.01$. We also deduce that the fraction of co-clustered IgE-FcεRI to total IgE-FcεRI is also 0.08, or 8% of total IgE-FcεRI complexes are preclustered with Lyn. These values are reported in Supplemental Table S1B. The cross-correlation functions thus allow stochiometries to be estimated, although we note that these numbers do not represent any populations of Lyn that are not labeled by gold-conjugated antibodies.

After as little as 1 min stimulation at 37 °C with antigen, IgE-FcεRI and Lyn become highly cross-correlated, extending to long distances (ξ_c = 86 nm), confirming that these proteins strongly co-cluster under these conditions (Figure 5B). The size of these co-clusters decreases with time, consistent with the decreasing cluster size observed with IgE-FcεRI and Lyn individually (Figures 3B and 4A), and fit parameters are reported in Supplemental Table S1B. The average number of proteins per co-cluster can be evaluated from cross-correlation functions, and stimulated values are very close to those obtained for IgE-FcεRI and Lyn in single label experiments (Supplemental Figure S1A,B), providing further support that these proteins are localized in the same co-clusters after antigen stimulation. Consistent with the visual impression in Figure 5A, cross-correlation functions show that IgE-FcεRI and Thy-1 do not significantly co-cluster in either unstimulated or stimulated cells (Figure 4, yellow triangles, and Figure 5B, cyan circles, respectively).

Stimulated Co-clustering of IgE-FcεRI and Lyn Depends on Both Tyrosine Kinase Activity and Membrane Cholesterol. To elucidate the structural basis for the co-clustering of Lyn with antigen-cross-linked IgE-FcεRI, we investigated the effects of treatments known to perturb membrane structure and function. In one set of experiments, we evaluated the role of phosphorylation-dependent protein−protein interactions between IgE-FcεRI and Lyn using the Src-family kinase inhibitor PP1 to inhibit Lyn kinase activity.[39] Figure 6A, top two panels, shows representative SEM images of IgE and Lyn after 1 min of antigen stimulation both with and without 4 μM PP1 (or other treatments described below). Many images of these samples

dx.doi.org/10.1021/jp300197p | J. Phys. Chem. B 2012, 116, 6923−6935

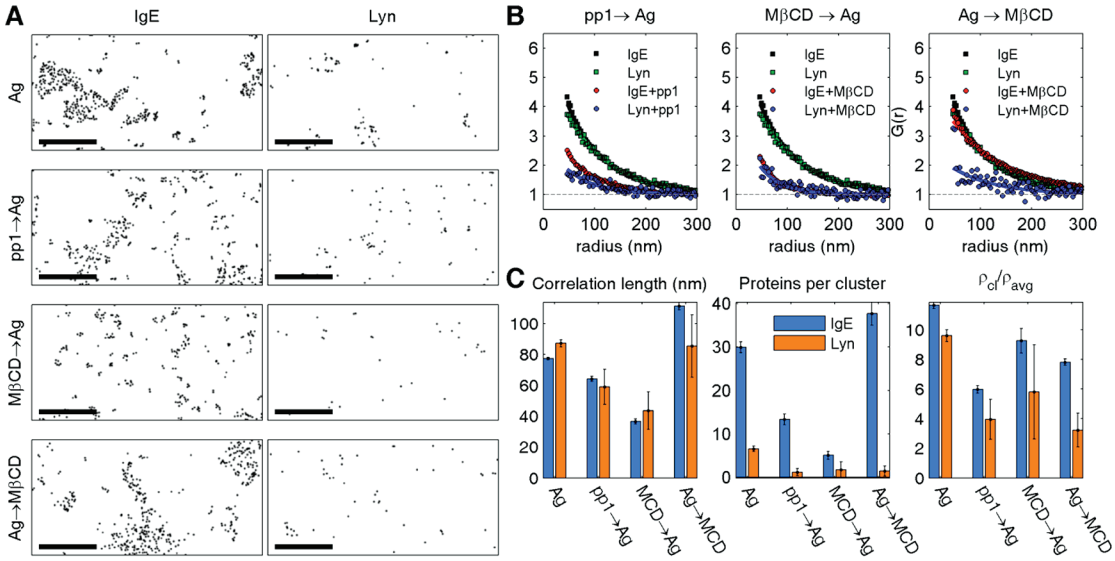

Figure 6. Co-redistribution of Lyn with cross-linked IgE-FcεRI is sensitive to Src family kinase activity and plasma membrane cholesterol levels. (A) Representative reconstructed BSD images of immuno-gold labeled IgE-FcεRI and Lyn in antigen stimulated cells and parallel samples treated with PP1 prior to stimulation or with MβCD either before or after stimulation. Scale bar is 500 nm. (B) Autocorrelation functions quantify particle distributions from many images in experiments represented in (A), and curves are fit to exponentials for $r > 50$ nm as in Figure 3 (solid lines). (C) Parameters ξ, N_{cl}, and ρ_{cl}/ρ are extracted from fits shown in panel B; values are tabulated in Supplemental Table S1C.

from multiple experiments were evaluated with autocorrelation functions (Figure 6B, left panel) that are well fit in all cases by single exponential functions (solid lines in 6B), providing useful parameters of protein clustering: correlation length (ξ), number of gold particles labeling proteins per cluster (N_{cl}), and ratio of gold particle density in clusters to average surface density (ρ_{cl}/ρ) (Figure 6C). Values for these parameters are reported in Supplemental Table S1C.

When the tyrosine kinase inhibitor PP1 is added to cells prior to stimulation, large clusters of both IgE and Lyn still result from antigen cross-linking of IgE-FcεRI (values of ξ decrease by less than 30% compared to no PP1; Figure 6C, left panel). However, values of N_{cl} decrease substantially in the presence of PP1: For IgE, N_{cl} decreases by ∼55%; for Lyn, N_{cl} decreases by ∼80% (Figure 6C, middle panel). Consistent with this, values of ρ_{cl}/ρ for both IgE-FcεRI and Lyn in clusters decrease after PP1 treatment (Figure 6C, right panel). These results indicate that tyrosine kinase activity of Lyn, including phosphorylation of FcεRI, plays a significant role in the accumulation of both IgE-FcεRI and Lyn in these antigen stimulated clusters.

We investigated the role of plasma membrane domains in modulating IgE-FcεRI and Lyn protein distributions by reducing membrane cholesterol with 10 mM MβCD for 5 min at 37 °C, either before or after addition of antigen. As visualized in Figure 6A (third panel from top) and quantified with autocorrelation functions for many images in Figure 6B,C, addition of MβCD prior to antigen cross-linking results in decrease of cluster size for both IgE-FcεRI and Lyn (ξ decreases by ∼50% for both; Figure 6C, left panel), and the N_{cl} are decreased by even larger amounts (∼80% reduction for both; Figure 6C, middle panel). We found that FcεRI-Lyn co-localization observed in resting cells (Figure 5B) also decreases slightly with reduced cholesterol levels in double label experiments (Supplemental Figure S4B). These results are consistent with the presence of cholesterol-dependent membrane domains that enhance the clustering of IgE-FcεRI initiated by antigen cross-linking, and this membrane structure also increases co-clustering of IgE-FcεRI and Lyn.

If cells are treated with MβCD for 5 min after addition of antigen for 1 min, the cluster sizes determined for IgE-FcεRI and Lyn do not change dramatically compared to 5 min stimulation in the absence of MβCD (Figure 6C, left panel). Interestingly, however, the N_{cl} decreases much more for Lyn (∼70%) than for IgE-FcεRI (∼10%; Figure 6C, middle panel). Cholesterol reduction also decreases the ρ_{cl}/ρ for both IgE-FcεRI and Lyn when MβCD is added either before or after antigen (Figure 6C, right panel). These effects of cholesterol reduction indicate that plasma membrane lipids contribute both to the structural organization of antigen stimulated IgE-FcεRI clustering and to the coupling of clustered IgE-FcεRI with Lyn kinase during initial stages of signal transduction.

DISCUSSION

The methodological advances of our SEM measurements with pair correlation analysis provide a quantitative description of, and nanoscale insight into, IgE-FcεRI-mediated redistributions of signaling proteins in the plasma membranes of RBL mast cells. We find that stimulation of cells by antigen cross-linking of IgE-FcεRI causes co-redistribution of Lyn kinase within a minute, and that the size and densities of these clusters depend on both tyrosine kinase activity and cholesterol-dependent membrane structure. Syk and LAT form clusters of sizes similar to those of IgE-FcεRI and Lyn and have similar spatial properties over 20 min stimulation time, indicating that all of these proteins occupy the same membrane domains. By contrast, Thy-1 does not co-redistribute with clustered IgE-FcεRI.

Enabling SEM Methodology and Analysis. Our study used a combination of SED and BSD in SEM images of intact cells to characterize redistributions of both outer and inner leaflet signaling proteins that are immuno-gold labeled following sufficient fixation (4% paraformaldehyde, 0.1% glutaraldehyde) to prevent antibody-induced protein redistributions.[40] BSD yields an image of gold particle distributions on the cell surface. SED evaluates membrane topography,

dx.doi.org/10.1021/jp300197p | J. Phys. Chem. B 2012, 116, 6923−6935

providing a check on apparent heterogeneity of gold particles that may be due to morphological irregularities. Previous TEM studies of osmium stained, plasma membrane sheets ripped from RBL cells had concluded that neither IgE-FcεRI nor Lyn are randomly distributed in unstimulated cells and that antigen cross-linking causes only limited association of Lyn with larger IgE-FcεRI clusters.[27,28] Discrepancies between our results and those previous reports may be due in part to their evaluation of membrane sheet preparations and use of lighter fixation conditions, as well as other factors. We chose to evaluate intact cells to avoid perturbation of membrane/cytoskeletal interactions occurring during extraction of membrane sheets, which have previously been shown to impact protein reorganization.[41,42]

Other features that strengthen our methodology and validate our nanoscale view of IgE-FcεRI-initiated membrane redistributions include specific immuno-labeling of target proteins (Supplemental Figure S2) and automated image analysis (Figure 1 and Supplemental Figure S1). A possible limitation to any scheme for labeling cellular components is accessibility of the target protein. In our studies, IgE (bound to FcεRI) and Thy-1 on the cell surface are probably completely accessible to the labeling antibodies, and our measurement of ρ is consistent with expected FcεRI surface density (Table 1;[34]). To obviate a common problem of loss of immunoreactivity of proteins at the extracellular surface of strongly fixed cells, our labeling scheme takes advantage of primary antibodies that are specific for small molecules (anti-Alexa488 to label Alexa488-IgE) or are otherwise known to bind after fixation (mAb OX7 to label Thy1). Target proteins labeled on the cytoplasmic side may not be completely accessible (or immunoreactive), and correspondingly our ρ values for Lyn, Syk, and LAT may be lower limits. For all of these target proteins, the accessible proteins have a labeling efficiency of ~1 gold particle per target (Table 1, Supplemental Figure S3) corresponding to a good statistical sampling of the labeled populations. We carry out quantitative evaluation of large data sets of particle coordinates with pair auto- and cross-correlation functions (e.g., Figures 4−6, Supplemental Table S1), which measure increased densities (compared to random distributions) as a function of radial distance away from an average particle. Correspondingly, the size of clusters is given by the decay of the curve (i.e., how steeply $g(r)$ or $c(r)$ decreases with r), and the number of particles in an average cluster can be calculated (see Experimental Methods).

A pitfall of immuno-labeling in nanoresolution images is multiple labels binding to single target proteins. This overcounting can lead to misinterpreting the data as short-range self-clustering of the target protein. We have shown how overcounting in electron and super-resolution fluorescence micrographs can be identified and estimated with pair correlation functions.[35] This potential artifact can be avoided if a labeling scheme is employed that ensures only a single gold label can bind to a target protein, or when two pools of functionally identical target proteins are labeled with distinguishable probes (as shown in Figure 2D). However, these labeling strategies are often not practical, as was the case for the majority of experiments conducted in this study. For the purposes of our present work, we instead avoided this potential artifact in single label experiments by considering the autocorrelation curves at radial distances >50 nm, which evaluate clusters beyond the dimensions of target protein and labeling antibodies (Figure 2 and Supplemental Figure S3). At these distances, the autocorrelation curves are well fit by single exponential functions (e.g., Figures 3 and 6 and Supplemental Figure S3B) that allow simple characterization of clusters with physical parameters: correlation length (ξ), number of gold particles in the cluster (N_{cl}), and density of gold particles in the cluster (ρ_{cl}) that can be compared to the overall average surface density (ρ_{cl}/ρ) (Figure 4, Supplemental Tables S1A and C). Double-label experiments are characterized with cross-correlation curves that are not affected by overcounting. These curves can also be fit with single exponential functions, yielding ξ_{cl} as a measure of size for the co-cluster (Figure 5, Supplemental Table S1B).

Although mathematically related, we find that pair correlation functions have significant advantages over Ripley's functions that are commonly used for image analysis in electron microscopy and in super resolution fluorescence localization microscopy. Ripley's functions can be disadvantageous because they are generated by integrating correlation functions, and consequently short-radii contributions (e.g., steric limitations of finite-sized gold particles or multiple gold labels on individual target proteins) are propagated to long radii, which may introduce errors.[35] Consequently, it is more difficult to interpret measured distributions with appropriate accounting for these experimental limitations. Even in the absence of these potential artifacts, it can be more difficult to extract physical parameters such as domain size from Ripley's functions.[43] Collectively, the methodology and analysis we developed for this study improve the fidelity with which EM measurement of immuno-gold labeled proteins reports physiologically relevant, nanoscale distributions of plasma membrane proteins.

Quantitative Nanoscale View of Stimulated Protein Redistribution to Initiate Signaling. We find that each of IgE-FcεRI, Lyn, Syk, and LAT are randomly dispersed over distances greater than 50 nm in unstimulated cells. After 1 min of cross-linking IgE-FcεRI with multivalent antigen at 37 °C, each redistributes into large clusters. Each of these stimulated clusters have ξ values in the range of 70−90 nm (Figures 3B and 4A). In double-label experiments, IgE-FcεRI and Lyn show limited pairing in unstimulated cells (ξ_c < 10 nm), and they co-redistribute within the same large clusters (ξ_c~85 nm) after 1 min of antigen stimulation (Figure 5B). Our observations of cross-linked IgE-FcεRI and Lyn co-clustering contrasts with previous results in which Lyn was observed to be largely segregated from cross-linked IgE-FcεRI that co-clusters with Syk.[27] We investigated the possibility that Lyn might segregate away from IgE-FcεRI at longer stimulation times, but we observed that co-clustering persists even after 20 min of stimulation (Figure 5). Our results provide direct evidence for stable nanoscale association of Lyn with cross-linked FcεRI on a time scale that is consistent with the persistent signaling needed for sustained Ca^{2+} mobilization and granule exocytosis. Syk and LAT (but not Thy-1) also form clusters with properties similar to those of IgE-FcεRI and Lyn after antigen cross-linking (Figure 4). Changes in ρ_{cl}/ρ over 20 min suggest that membrane protein interactions within signaling clusters continue to change as stimulation progresses.

The structural basis for the molecular rearrangements that proceed from antigen cross-linking of IgE-FcεRI to initiate the earliest stages of transmembrane signaling have remained elusive because of experimental approaches with limited spatial or temporal resolution. As described in the Introduction section, the initial functional coupling between cross-linked IgE-FcεRI and Lyn kinase has been investigated with a variety

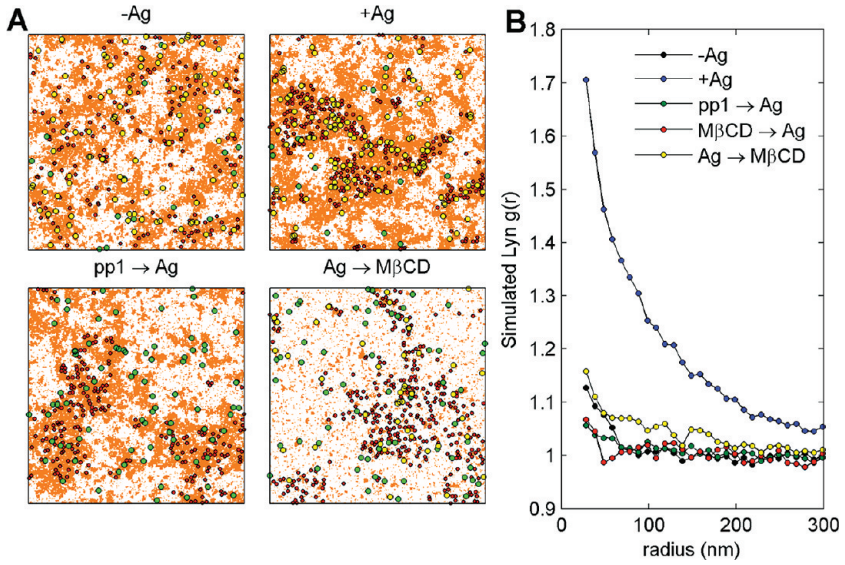

Figure 7. Lyn clustering is qualitatively reproduced using a minimal model that incorporates composition fluctuations and a Lyn activation state that depends on the local membrane environment. (A) Snapshots from simulations incorporating fluctuations of liquid-ordered (orange pixels) and liquid-disordered (white pixels) membrane regions, IgE-FcεRI complexes (small red circles), and Lyn in an active (yellow circles) or inactive (green circles) state. IgE-FcεRI distributions are fixed throughout the simulation and are taken from the images shown in Figure 6. Orange, ordered domains localize around clustered IgE-FcεRI receptors because cross-linked receptors prefer to partition into ordered regions. Lyn is allowed to move and also partitions into ordered regions. In addition, Lyn can be in two distinct states depending on local lipid environment. Lyn is in an active state when surrounded by liquid-ordered components, and experiences a strong binding affinity for IgE-FcεRI. Otherwise, Lyn is inactive and interacts weakly with IgE-FcεRI. A detailed description of the model and its implementation is provided in the Experimental Methods section. Lyn is nearly randomly distributed in unstimulated cells (−Ag). In simulations of antigen (+Ag) treated cells, most Lyn is activated and associated with receptors. In simulations of PP1-treated cells, Lyn is restricted to be in an inactive state (independent of its local environment), and fewer Lyn proteins partition into IgE-FcεRI rich clusters due to the absence of strong direct binding between components. The fraction of liquid-ordered membrane is reduced in simulations of MβCD-treated cells. Few Lyn proteins are activated or bound to receptor because Lyn is rarely surrounded by liquid-ordered components. As a result, Lyn is only weakly localized within receptor-rich domains. (B) Pair correlation functions for simulated Lyn proteins are calculated from 50 snapshots like those shown in A. Lyn is most strongly clustered in simulations with clustered receptors, and clustering is reduced in simulations mimicking cells treated with PP1 or MβCD.

of biochemical approaches, with some studies pointing to the importance of tyrosine phosphorylation and others to the importance of cholesterol-dependent membrane domains. With parallel SEM experiments we were able to nanoscopically visualize the effects of both membrane structure perturbation by cholesterol reduction and inhibition of Lyn-mediated tyrosine phosphorylation by PP1 on antigen-stimulated co-redistribution of IgE-FcεRI and Lyn.

As summarized in Figure 6, we found that reducing plasma membrane levels of cholesterol prior to multivalent antigen stimulation causes a decrease in the size (ξ) of Lyn and cross-linked IgE-FcεRI clusters, as well as a decrease in the number of both proteins in clusters (N_{cl}). Interestingly, cholesterol reduction after stimulation does not significantly change the size of IgE-FcεRI and Lyn clusters, but rather, the number of Lyn proteins present in stimulated clusters is substantially decreased. These results support the importance of cholesterol-dependent membrane structure in ongoing coupling between Lyn and cross-linked IgE-FcεRI. Cholesterol is important for maintaining the ordering of lipids (liquid-order-like phase behavior), and these domains interact with the cytoskeleton, such that effects of cholesterol reduction may be complex.[15] In unstimulated cells we found that cholesterol reduction decreases the small amount of cross-correlation between IgE-FcεRI and Lyn (Supplemental Figure S4). If there are weak protein interactions between Lyn and IgE-FcεRI-β as detected previously[10] these appear to be enhanced by their coassociation within cholesterol-dependent membrane domains of small dimensions prior to antigen cross-linking.

Consistent with our SEM experiments, we previously showed that cholesterol depletion reduces association of both Lyn and cross-linked IgE-FcεRI with detergent-resistant membranes that are isolated from RBL cells. This effect correlates with inhibition of stimulated tyrosine phosphorylation in live cells, indicating participation of cholesterol-dependent ordered lipid membrane structure in these functional interactions.[44] In the present study, the conditions of cholesterol reduction by MβCD are milder (10 mM MβCD for 5 min vs 60 min in the previous study), and we do not expect that functional coupling between these proteins would be completely prevented under present conditions. We found that cholesterol reduction after antigen cross-linking does not affect the size of IgE-FcεRI clusters, but rather decreases Lyn co-clustering.

Pretreatment of cells with the Src-family kinase inhibitor, PP1, has only a small effect on cluster dimensions of cross-linked IgE-FcεRI and Lyn under stimulating conditions, but the N_{cl}, and the ρ_{cl}/ρ for both IgE-FcεRI and Lyn are significantly decreased by this treatment (Figure 6C, Supplemental Table S1C). Stimulated phosphorylation of ITAM tyrosine residues in the β subunit of FcεRI creates binding sites for Lyn SH2 domains.[12] However, in the absence of this phosphorylation, residual co-clustering of Lyn with IgE-FcεRI occurs, involving interactions within cholesterol-dependent membrane domains and possibly direct protein interactions.[10] It is notable that PP1 causes a decrease in the density of cross-linked IgE-FcεRI

dx.doi.org/10.1021/jp300197p | J. Phys. Chem. B 2012, 116, 6923−6935

clusters, because this indicates that IgE-FcεRI clustering is not simply a passive consequence of cross-linking by antigen. Thus, these results implicate for the first time an active role by Lyn kinase in the process of IgE-FcεRI clustering, and this may involve other cellular structures.

Figure 7 presents a model that illustrates a possible physical basis of Lyn enrichment in IgE-FcεRI rich clusters that is consistent with our SEM results and those from previous studies. This model assumes that membrane heterogeneity arises from composition fluctuations consistent with our previous observations of fluctuations in isolated plasma membrane vesicles,[32] but similar outcomes could be produced assuming another basis of heterogeneity, such as nanodomains or modulated phases. Our model also assumes that both IgE-FcεRI (small red circles) and Lyn (yellow or green circles) prefer cholesterol-dependent, ordered membrane regions (orange), that the activation state of Lyn is sensitive to its local membrane environment, and that active Lyn (yellow circles) has enhanced protein−protein interactions with IgE-FcεRI. In antigen stimulated cells, this model predicts that Lyn will partition strongly into IgE-FcεRI-rich domains because both proteins prefer to partition into the same local membrane environment and because an ordered membrane environment promotes activation of Lyn, leading to phosphorylation and higher affinity binding between Lyn and FcεRI.

Consistent with our SEM results, this model predicts that the perturbations caused by PP1 and MβCD will decrease the partitioning of Lyn into IgE-FcεRI-rich clusters. We mimic PP1 addition by constraining Lyn to be in an inactive (green) state. As a consequence, Lyn is only slightly enriched in IgE-FcεRI rich clusters because the enhanced interactions between Lyn and FcεRI are prevented. This occurs even though both Lyn and IgE-FcεRI prefer the same local lipid environment because lipid-mediated interactions are weak, and there are many ordered membrane regions localized outside clustered receptors. We mimic cholesterol reduction by decreasing the surface fraction of ordered (orange) regions in the membrane. As a consequence, the clustering of receptors no longer stabilizes the relatively large, ordered domain. This results in there being less activated Lyn close to the receptors as well as a reduced lifetime of Lyn-FcεRI binding. Correlation functions from these simulations are in good qualitative agreement with experimental findings, and quantitative differences could arise from the overly simplistic nature of this model. This model is similar to the one we presented recently to describe coupling between cytoskeleton and the membrane,[31] and the simulation is further described in the Experimental Methods.

Collectively, our findings indicate that both cholesterol-dependent membrane lipid structure and phosphorylation-dependent protein−protein interactions mediate protein organization within the membrane after antigen stimulation and during the consequent IgE-FcεRI signaling response. These results are consistent with the hypothesis that ordered membrane domains facilitate selective protein partitioning within the same compartment and thereby stabilize functional interactions among these proteins and with other cellular structures.[15] Inhibition (by PP1) of FcεRI phosphorylation by Lyn may also result in loss of cytoskeletal interactions that further regulate stimulation-dependent co-clustering of IgE-FcεRI and Lyn. We previously showed that the actin cytoskeleton is involved in micrometer-scale co-redistribution of Lyn with clustered IgE-FcεRI,[18] and that actin-binding focal adhesion proteins also co-cluster, independent of integrins.[45] This may be a mechanism for connecting the phosphorylated receptor clusters to the actin cytoskeleton at later stages of signaling. Lyn-based attachment to the cytoskeleton may also be involved in Lyn co-clustering with IgE-FcεRI that we observe with SEM at shorter times and higher resolution. Interactions with the cytoskeleton contribute to restricted diffusion of cross-linked IgE-FcεRI, and may negatively regulate FcεRI signaling.[46]

CONCLUSIONS

Our study demonstrates that SEM with SED and BSD is valuable for investigating distributions of immuno-gold labeled signaling proteins on both outer and inner leaflets of plasma membrane of fixed, intact cells. Using pair correlation functions, we find that the proteins we investigated are randomly distributed over distances greater than 50 nm, and self-clustering observed at shorter radii cannot be distinguished from multiple gold labeling. Single-label experiments show that IgE-FcεRI, Lyn, Syk, and LAT all redistribute into clusters within 1 min of stimulation by multivalent antigen at 37 °C, and they remain clustered at longer stimulation times. Double-label experiments show that IgE-FcεRI and Lyn co-redistribute into clusters that are similar in size and persistence to those visualized in single label experiments over the same time-course. We also demonstrate that antigen-induced IgE-FcεRI and Lyn co-clustering is sensitive to inhibition of Lyn kinase activity and to changes in membrane domain structure caused by cholesterol reduction. These studies provide new insights into the mechanism of stimulation-dependent reorganization of IgE-FcεRI and associated signaling proteins that occurs on the nanoscale within minutes after antigen cross-linking. Mechanisms by which cytoskeletal interactions play an active role in regulating the heterogeneity of plasma membrane composition and antigen-stimulated IgE-FcεRI signaling assemblies represent important unanswered questions.

ASSOCIATED CONTENT

Supporting Information

We describe image processing: Supplemental Figure S1 shows how gold particle centers are identified using automated image processing algorithms. We describe labeling controls for these experiments: Figure S2 shows that gold labeling of target proteins used in these experiments is specific. We describe how measured clustering of gold particles at short distances is consistent with multiple gold labels on single target proteins: Figure S3 shows that self-clustering at short distances corresponds to overcounting of single labeled proteins. We describe the effect of cholesterol on co-clustering of FcεRI and Lyn in unstimulated cells: Figure S4 shows that FcεRI and Lyn are significantly co-clustered in unstimulated cells, with some dependence on cholesterol. Supplemental Table S1 tabulates fit parameter values from figures in the main text: Figure 3B, Figure 4, Figure 5B, and Figure 6C. This material is available free of charge via the Internet at http://pubs.acs.org.

AUTHOR INFORMATION

Corresponding Author

*Address: Department of Chemistry and Chemical Biology, Cornell University, Baker Laboratory, Ithaca, NY 14853-1301; phone: 607-255-4095; fax: 607-255-4137; e-mail: bab13@cornell.edu.

Present Addresses

[‡]University of Michigan, 930 N University, Ann Arbor, MI [§]48109.

[§]National Research Council, Washington, DC 20001.

[∥]NIH, CBMP/NICHD, 18 Library Dr., Bldg 18T, Rm101, Bethesda, MD 20892.

Author Contributions

[†]These authors contributed equally to this work.

Notes

The authors declare no competing financial interest.

■ ACKNOWLEDGMENTS

This research was supported by NIH Grant R01-AI018306 and by the Nanobiotechnology Center (NSF: ECS9876771). E.N.C. acknowledges support from the NIH (T32-GM08210) and Cornell's Tri-Institutional Training Program in Chemical Biology. S.L.V. acknowledges support from the NIH (K99GM087810) and the Miller Independent Scientist Program of Cornell's Department of Chemistry and Chemical Biology.

■ REFERENCES

(1) Blank, U.; Rivera, J. *Trends Immunol.* **2004**, *25*, 266−273.
(2) Kraft, S.; Kinet, J. P. *Nat. Rev. Immunol.* **2007**, *7*, 365−378.
(3) Siraganian, R. P.; Zhang, J.; Suzuki, K.; Sada, K. *Mol. Immunol.* **2002**, *38*, 1229−1233.
(4) Paolini, R.; Jouvin, M. H.; Kinet, J. P. *Nature* **1991**, *353*, 855−858.
(5) Odom, S.; Gomez, G.; Kovarova, M.; Furumoto, Y.; Ryan, J. J.; Wright, H. V.; Gonzalez-Espinosa, C.; Hibbs, M. L.; Harder, K. W.; Rivera, J. *J. Exp. Med.* **2004**, *199*, 1491−1502.
(6) Holowka, D.; Sil, D.; Torigoe, C.; Baird, B. *Immunol. Rev.* **2007**, *217*, 269−279.
(7) Sil, D.; Lee, J. B.; Luo, D.; Holowka, D.; Baird, B. *ACS Chem. Biol.* **2007**, *2*, 674−684.
(8) Pribluda, V. S.; Pribluda, C.; Metzger, H. *Proc. Natl. Acad. Sci. U.S.A.* **1994**, *91*, 11246−11250.
(9) Yamashita, T.; Mao, S. Y.; Metzger, H. *Proc. Natl. Acad. Sci. U.S.A.* **1994**, *91*, 11251−11255.
(10) Vonakis, B. M.; Chen, H.; Haleem-Smith, H.; Metzger, H. *J. Biol. Chem.* **1997**, *272*, 24072−24080.
(11) Furumoto, Y.; Nunomura, S.; Terada, T.; Rivera, J.; Ra, C. *J. Biol. Chem.* **2004**, *279*, 49177−49187.
(12) On, M.; Billingsley, J. M.; Jouvin, M. H.; Kinet, J. P. *J. Biol. Chem.* **2004**, *279*, 45782−45790.
(13) Young, R. M.; Zheng, X.; Holowka, D.; Baird, B. *J. Biol. Chem.* **2005**, *280*, 1230−1235.
(14) Gosse, J. A.; Wagenknecht-Wiesner, A.; Holowka, D.; Baird, B. *J. Immunol.* **2005**, *175*, 2123−2131.
(15) Holowka, D.; Gosse, J. A.; Hammond, A. T.; Han, X.; Sengupta, P.; Smith, N. L.; Wagenknecht-Wiesner, A.; Wu, M.; Young, R. M.; Baird, B. *Biochim. Biophys. Acta* **2005**, *1746*, 252−259.
(16) Holowka, D.; Sheets, E. D.; Baird, B. *J. Cell Sci.* **2000**, *113* (Pt 6), 1009−1019.
(17) Larson, D. R.; Gosse, J. A.; Holowka, D. A.; Baird, B. A.; Webb, W. W. *J. Cell Biol.* **2005**, *171*, 527−536.
(18) Wu, M.; Holowka, D.; Craighead, H. G.; Baird, B. *Proc. Natl. Acad. Sci. U.S.A.* **2004**, *101*, 13798−13803.
(19) Saitoh, S.; Arudchandran, R.; Manetz, T. S.; Zhang, W.; Sommers, C. L.; Love, P. E.; Rivera, J.; Samelson, L. E. *Immunity* **2000**, *12*, 525−535.
(20) Das, R.; Hammond, S.; Holowka, D.; Baird, B. *Biophys. J.* **2008**, *94*, 4996−5008.
(21) Rust, M. J.; Bates, M.; Zhuang, X. *Nat. Methods* **2006**, *3*, 793−795.
(22) Klar, T. A.; Jakobs, S.; Dyba, M.; Egner, A.; Hell, S. W. *Proc. Natl. Acad. Sci. U.S.A.* **2000**, *97*, 8206−8210.
(23) Hess, S. T.; Girirajan, T. P.; Mason, M. D. *Biophys. J.* **2006**, *91*, 4258−4272.
(24) Betzig, E.; Patterson, G. H.; Sougrat, R.; Lindwasser, O. W.; Olenych, S.; Bonifacino, J. S.; Davidson, M. W.; Lippincott-Schwartz, J.; Hess, H. F. *Science* **2006**, *313*, 1642−1645.
(25) Stump, R. F.; Pfeiffer, J. R.; Seagrave, J.; Oliver, J. M. *J. Histochem. Cytochem.* **1988**, *36*, 493−502.
(26) Seagrave, J.; Pfeiffer, J. R.; Wofsy, C.; Oliver, J. M. *J. Cell. Physiol.* **1991**, *148*, 139−151.
(27) Wilson, B. S.; Pfeiffer, J. R.; Oliver, J. M. *J. Cell Biol.* **2000**, *149*, 1131−1142.
(28) Wilson, B. S.; Pfeiffer, J. R.; Surviladze, Z.; Gaudet, E. A.; Oliver, J. M. *J. Cell Biol.* **2001**, *154*, 645−658.
(29) Zacharias, D. A.; Violin, J. D.; Newton, A. C.; Tsien, R. Y. *Science* **2002**, *296*, 913−916.
(30) Sengupta, P.; Hammond, A.; Holowka, D.; Baird, B. *Biochim. Biophys. Acta* **2008**, *1778*, 20−32.
(31) Machta, B. B.; Papanikolaou, S.; Sethna, J. P.; Veatch, S. L. *Biophys. J.* **2011**, *100*, 1668−1677.
(32) Veatch, S. L.; Cicuta, P.; Sengupta, P.; Honerkamp-Smith, A.; Holowka, D.; Baird, B. *ACS Chem. Biol.* **2008**, *3*, 287−293.
(33) Faeder, J. R.; Hlavacek, W. S.; Reischl, I.; Blinov, M. L.; Metzger, H.; Redondo, A.; Wofsy, C.; Goldstein, B. *J. Immunol.* **2003**, *170*, 3769−3781.
(34) Erickson, J.; Goldstein, B.; Holowka, D.; Baird, B. *Biophys. J.* **1987**, *52*, 657−662.
(35) Veatch, S. L.; Machta, B. B.; Shelby, S. A.; Chiang, E. N.; Holowka, D.; Baird, B. *PLoS ONE* **2012**, *7*, e31457.
(36) Mendoza, G.; Metzger, H. *Nature* **1976**, *264*, 548−550.
(37) Furuichi, K.; Rivera, J.; Isersky, C. *J. Immunol.* **1984**, *133*, 1513−1520.
(38) Paolini, R.; Molfetta, R.; Beitz, L. O.; Zhang, J.; Scharenberg, A. M.; Piccoli, M.; Frati, L.; Siraganian, R.; Santoni, A. *J. Biol. Chem.* **2002**, *277*, 36940−36947.
(39) Amoui, M.; Draber, P.; Draberova, L. *Eur. J. Immunol.* **1997**, *27*, 1881−1886.
(40) Tanaka, K. A.; Suzuki, K. G.; Shirai, Y. M.; Shibutani, S. T.; Miyahara, M. S.; Tsuboi, H.; Yahara, M.; Yoshimura, A.; Mayor, S.; Fujiwara, T. K.; Kusumi, A. *Nat. Methods* **2010**, *7*, 865−866.
(41) Elgsaeter, A.; Branton, D. *J. Cell Biol.* **1974**, *63*, 1018−1036.
(42) Ursitti, J. A.; Pumplin, D. W.; Wade, J. B.; Bloch, R. J. *Cell Motil. Cytoskeleton* **1991**, *19*, 227−243.
(43) Kiskowski, M. A.; Hancock, J. F.; Kenworthy, A. K. *Biophys. J.* **2009**, *97*, 1095−1103.
(44) Sheets, E. D.; Holowka, D.; Baird, B. *J. Cell Biol.* **1999**, *145*, 877−887.
(45) Torres, A. J.; Vasudevan, L.; Holowka, D.; Baird, B. A. *Proc. Natl. Acad. Sci. U.S.A.* **2008**, *105*, 17238−17244.
(46) Andrews, N. L.; Lidke, K. A.; Pfeiffer, J. R.; Burns, A. R.; Wilson, B. S.; Oliver, J. M.; Lidke, D. S. *Nat. Cell Biol.* **2008**, *10*, 955−963.